Polyclonal Secondary FGFR2 Mutations Drive Acquired Resistance to FGFR Inhibition in Patients with FGFR2 Fusion-Positive Cholangiocarcinoma

Goyal, Lipika; Saha, Supriya K; Liu, Leah Y; Siravegna, Giulia; Leshchiner, Ignaty; Ahronian, Leanne G; Lennerz, Jochen K; Vu, Phuong; Deshpande, Vikram; Kambadakone, Avinash; Mussolin, Benedetta; Reyes, Stephanie; Henderson, Laura; Sun, Jiaoyuan Elisabeth; Van Seventer, Emily E; Gurski, Joseph M; Baltschukat, Sabrina; Schacher-Engstler, Barbara; Barys, Louise; Stamm, Christelle; Furet, Pascal; Ryan, David P; Stone, James R; Iafrate, A John; Getz, Gad; Graus Porta, Diana; Tiedt, Ralph; Bardelli, Alberto; Juric, Dejan; Corcoran, Ryan B; Bardeesy, Nabeel; Zhu, Andrew X. Polyclonal Secondary FGFR2 Mutations Drive Acquired Resistance to FGFR Inhibition in Patients with FGFR2 Fusion-Positive Cholangiocarcinoma. CANCER DISCOVERY. None pp: CD-16-1000-0.
DOI: 10.1158/2159-8290.CD-16-1000

Polyclonal secondary FGFR2 mutations drive acquired resistance to FGFR inhibition in FGFR2 fusion-positive cholangiocarcinoma patients

Lipika Goyal[1,*], Supriya K. Saha[1,#,*], Leah Y. Liu[1], Giulia Siravegna[2,3], Ignaty Leshchiner[4], Leanne G. Ahronian[1], Jochen K. Lennerz[5], Phuong Vu[1], Vikram Deshpande[5], Avinash Kambadokone[6], Benedetta Mussolin[2,3], Stephanie Reyes[1], Laura Henderson, J. Elisabeth Sun, Emily E. Van Seventer, Joseph M. Gurski Jr[1], Sabrina Baltschukat, Barbara Schacher-Engstler, Louise Barys, Pascal Furet, David P. Ryan[1], James R. Stone, A. John Iafrate[5], Gad Getz[1], Diana Graus Porta, Ralph Tiedt, Alberto Bardelli[2,3], Dejan Juric[1], Ryan B. Corcoran[1,¶], Nabeel Bardeesy[1,¶], Andrew X. Zhu[1,¶]

[1]Massachusetts General Hospital Cancer Center, Harvard Medical School, Boston, MA 02114, USA;
[2]Candiolo Cancer Institute-FPO, IRCCS, Candiolo, Torino, Italy 10060;
[3]Department of Oncology, University of Torino, Torino, Italy 10060;
[4]Broad Institute of Massachusetts Institute of Technology and Harvard, Cambridge, MA 02142, USA
[5]Department of Pathology, Massachusetts General Hospital, Boston, MA 02114, USA.
[6]Department of Radiology, Massachusetts General Hospital, Boston, MA 02114, USA;
Novartis XXXXX.

*L. Goyal and S. Saha contributed equally to this work

Present address: Fred Hutchinson Cancer Research Center, 1100 Fairview Ave. N., Mail Stop C1-167, Seattle, WA 98109

Running Title: Acquired FGFR2 resistanc e mutations in cholangiocarcinoma

Keywords: BGJ398, Fibroblast Growth Factor Receptor, Intrahepatic Cholangiocarcinoma, Resistance Mutations, cell free DNA

Financial Support: L.G. is supported by a,Massachusetts General Hospital (MGH) Executive Committee on Research Fund for Medical Discovery Award, Cholangiocarcinoma Foundation Research Fellowship, and NIH Loan Repayment Program Grant. S.K.S. is supported by a NCI Mentored Clinical Scientist Research Career Development Award (1K08CA194268-01). D.J. is supported by the HMS Laboratory for Systems Pharmacology Grant (P50GM107618) and the Susan Eid Tumor Heterogeneity Initiative. N.B. is the holder of the Gallagher Chair in Gastrointestinal Cancer Research at MGH. N.B. and A.Z. are supported by the TargetCancer Foundation and by a Translational Research Grant Award from V Foundation for Cancer Research. This work was also supported by grants from the NIH/NCI Gastrointestinal Cancer SPORE P50 CA127003 (to L.G., S.K.S, R.B.C, and N.B.). R.B.C acknowledges support from a Damon Runyon Clinical Investigator Award and NIH/NCI 1K08CA166510 (all to R.B.C.). L.G., N.B., and A.Z. are supported by the Jonathan Kraft Translational Award.

¶ Corresponding Authors:

Andrew X. Zhu, MD, PhD, Massachusetts General Hospital Cancer Center, 55 Fruit Street, LH/POB 232, Boston, MA 02114-2698. Phone: 617-643-3415; Fax: 617-724-3166; E-mail: AZHU@PARTNERS.ORG

Nabeel Bardeesy, Massachusetts General Hospital, 185 Cambridge Street, CPZN 4216, Boston, MA 02114. Phone: 617-643-2579; Fax: 617-643-3170; E-mail: nbardeesy@partners.org

Ryan B. Corcoran, Massachusetts General Hospital Cancer Center, 149 13th Street, 7th Floor, Boston, MA 02129. Phone: 617-726-8599; Fax: 617-643-0798; E-mail: rbcorcoran@partners.org

Conflicts of Interest: R.B.C. has received research funding from AstraZeneca and is a consultant/advisory board member for Genentech, Merrimack Pharmaceuticals, Astex Pharmaceuticals, N-of-one, Taiho Pharmaceuticals, and Avidity Biosciences. D.J. has received research funding from Novartis and is a consultant/advisory board member for Novartis, EMD Serono, Natera and Eisai. A.Z. has received research funding from Novartis and Lilly and is a consultant/advisory board member for Novartis. XX, YY, XX are employees and shareholders of Novartis. All other authors have no conflicts to disclose.

Abstract

Genetic alterations in the fibroblast growth factor receptor (FGFR) pathway are promising therapeutic targets in many cancers, including intrahepatic cholangiocarcinoma (ICC). The FGFR inhibitor BGJ398 displayed encouraging efficacy in patients with FGFR2 fusion-positive ICC in a phase II trial, although responses were not durable. Here, we report the molecular basis for acquired resistance to BGJ398 in three patients via integrative genomic characterization of cell-free circulating tumor DNA (cfDNA), primary tumors, and metastases. Serial analysis of cfDNA demonstrated multiple recurrent point mutations in the FGFR2 kinase domain at progression. Accordingly, biopsy of post-progression lesions and rapid autopsy revealed marked inter- and intra-tumoral heterogeneity, with different FGFR2 mutations in individual resistant clones. Molecular modeling and *in vitro* studies indicated that each mutation leads to BGJ398 insensitivity and is surmountable by structurally distinct FGFR inhibitors. Thus, polyclonal secondary FGFR2 mutations represent an important clinical resistance mechanism that may inform development of future therapeutic strategies.

Significance

We report the first genetic mechanisms of clinical acquired resistance to FGFR inhibition in FGFR2 fusion-positive ICC patients. Our findings can inform future strategies for detecting resistance mechanisms and inducing more durable remissions in ICC and in the wide variety of cancers where the FGFR pathway is being explored as a therapeutic target.

Introduction

The FGFR pathway includes a family of 22 polypeptide ligands (FGFs) and 4 receptor tyrosine kinases (FGFRs) which regulate diverse physiologic processes [reviewed in (1)]. FGFR signaling is activated through recurrent gain-of-function mutations, chromosomal translocations, and amplifications in a variety of cancers including squamous non-small cell lung cancers, head and neck squamous cell carcinomas, breast cancers, urothelial carcinomas, and intrahepatic cholangiocarcinomas (ICCs) [reviewed in (2)]. Thus, the recent clinical development of potent and selective FGFR kinase inhibitors has opened a promising therapeutic avenue in many previously intractable malignancies.

Genetic lesions that activate FGFR2 are particularly common in ICC, a malignancy of the intrahepatic bile ducts that has been rising in incidence both in the United States and globally for decades (3, 4). As an aggressive tumor originating in the liver, ICC often remains asymptomatic until reaching an advanced stage, precluding curative therapy in a majority of cases. Palliative chemotherapy with gemcitabine and a platinum agent offers patients with unresectable or metastatic disease a median survival of less than one year (5). While no targeted agents are currently approved in ICC, the recent discovery of FGFR2 fusions in an estimated 10-20% of patients stands to change the therapeutic paradigm in this disease. Multiple fusion partners have been identified, including BICC1, AHCYL1, TACC3, MGEA5, and PPHLN1 (6-12). In most cases, the 5' exons 1-17 of FGFR2, containing the intact kinase domain, are fused in-frame to a 3' partner. The chimeric proteins are believed to undergo ligand-independent receptor dimerization leading to engagement of multiple downstream oncogenic pathways including MAPK and PI3K/AKT signaling (13).

The oral, selective, and ATP-competitive pan-FGFR inhibitor BGJ398 has demonstrated anti-tumor activity in preclinical models harboring FGFR genetic alterations (14, 15). This agent is currently being tested in a phase II multicenter trial in patients with advanced cholangiocarcinoma with FGFR aberrations who have progressed on first line chemotherapy.

The reported preliminary data from this trial highlight an impressive objective response rate of 21% and a median time on treatment of 188 days (16). This efficacy of targeted therapy beyond the first line in ICC is unprecedented. However, as seen with other targeted therapies and kinase inhibitors in particular (17, 18), acquired resistance inevitably develops.

Here, we present the integrative molecular analysis of cell-free circulating tumor DNA (cfDNA), primary tumors, and metastases to define the acquired resistance mechanisms to BGJ398 in three patients with advanced FGFR2-fusion+ ICC. These combined analyses revealed the emergence of secondary kinase mutations that confer BGJ398 insensitivity in each patient at the time of progression. A striking degree of inter-tumoral heterogeneity was observed, with distinct FGFR2 point mutations identified in different metastases from the same patient. Overall, these data suggest that secondary FGFR2 kinase domain mutations are an important mechanism of clinical acquired resistance to FGFR inhibitors, and that next-generation inhibitors capable of overcoming these resistance mutations may be important future clinical strategies for these cancers.

Results

Clinical acquired resistance to BGJ398

Three patients with FGFR2-fusion+ ICC were treated on the phase II trial of BGJ398 (NCT02150967), and serial cfDNA samples and tumor biopsies were subject to genomic analysis. Patient #1 presented at age 59 years old with an unresectable ICC, and was initially treated with gemcitabine and cisplatin for 10 months. Molecular testing of the tumor with the Solid Fusion Assay (SFA), a clinical test capable of detecting fusion events in over 50 cancer-related genes (19), revealed an FGFR2-ZYMY4 fusion. Following progression on chemotherapy, the patient underwent a repeat liver biopsy (Pre-treatment) and then initiated treatment on BGJ398. The patient achieved a -40.6% response by RECISTv1.1 criteria at 2 months and a -49.9% response at four months (Figure 1A, *left-upper panel and right panel*).

However, the 6 month CT scan showed a mixed response with progression of 2 satellite left lobe lesions. The patient's CA19-9 decreased from 242 to 48, and then rose to 156 U/mL during this time (Figure 1A, *left-upper panel*).

Patient #2 underwent a left hepatectomy at age 47 years old for a 10.9 cm, T2N0 ICC, and received adjuvant chemotherapy. Five months later, the patient developed a solitary biopsy-proven liver metastasis (Pre-treatment) and multiple subcentimeter bilateral pulmonary metastases. As SFA testing revealed an FGFR2-OPTN fusion, the patient was then enrolled in the BGJ398 trial, achieving a maximum response of -28% at 2 months (Figure 1B, *left-upper panel and right panel*). Unfortunately, the 4 month CT scan revealed a mixed response with a new 1.3 cm lesion appearing in the dome of the liver. The CA19-9 also initially decreased from 57 to 17, but then increased marginally to 21 U/mL during this period (Figure 1B, *left-upper panel*). The patient passed away 3 months later.

Patient #3 presented at age 43 years old with a 7 cm ICC involving the right hepatic lobe with metastases to the lymph nodes and lungs, which progressed through initial palliative chemotherapy. SFA testing revealed an FGFR2-BICC1 fusion. The patient enrolled in the BGJ398 trial and achieved a response of -28.4% at 2 months and a maximum response of -36.9% at 6 months. Unfortunately, the 8 month scan showed a mixed response with growth of multiple liver lesions and lymph nodes (Figure 1C, left-upper panel and right panel).

Detection of secondary FGFR2 resistance mutations in cfDNA

To identify potential mechanisms of acquired resistance, we analyzed pre-treatment and post-progression cfDNA from all three patients for mutations and copy number alterations in 70 cancer-related genes using the next-generation sequencing (NGS)-based Guardant360 assay (20). Remarkably, analysis of the post-progression cfDNA from Patient #1 showed five independent point mutations in FGFR2 (N549H, N549K, V564F, E565A and K659M), none of which were detected in the baseline plasma (Figure 1A, *right panel*). Similarly, analysis of

cfDNA from Patient #2 also revealed five distinct FGFR2 point mutations (N549H, V564F, E565A, L617V, and K641R) exclusively in post-progression specimens (Figure 1B*, right panel*). Finally, cfDNA from Patient #3, who continued on therapy for the longest period of time, contained a single FGFR2 point mutation (V564F) at the time of progression (Figure 1C*, right panels*).

We monitored the relative levels of specific mutations in cfDNA in a set of serially collected plasma samples from patients #1 and 2 (N=5 and 4 samples, respectively) using droplet digital PCR (ddPCR). Since detection of gene fusions across all cfDNA specimens is technically challenging, we examined 'truncal' mutations identified by whole-exome sequencing of pre-treatment tumor biopsy as a surrogate for overall tumor burden in cfDNA (ARID2 I200T in Patient #1 and PBRM1 R710* in Patient #2). Both alterations decreased initially with treatment but rose with disease progression (Figure 1A and B, *lower-left panels*). By contrast, FGFR2 point mutations were not detected at baseline, but each rose at 2 to 6 months after response, coincident with clinical progression. In Patient #3, NGS analysis of cfDNA using the Guardant360 assay was able to detect this specific FGFR2-BICC1 fusion in each of three serial samples collected, and revealed a decrease upon initiation of BGJ398, but an increase at the time of progression. This increase coincided with the detection of the FGFR2 V564F mutation (Figure 1C, *lower-left panel*). The development of secondary FGFR2 kinase domain mutations in all three patients, suggests that such mutations are an important mechanism of acquired resistance to FGFR inhibition.

Whole exome and RNA sequencing of serial tumor biopsies

Paired pre-treatment and post-progression biopsy samples available from Patients #1 and #2 were analyzed by whole-exome sequencing (WES) and RNA sequencing to determine intratumoral genomic changes. Importantly, RNA sequencing confirmed the presence of the fusion alleles in the post-progression biopsies in both cases (Patient #1, FGFR2-ZMYMY4;

Patient #2, FGFR2-OPTN) (Figures 1A and B, *right panels*), suggesting that clinical progression resulted from the acquisition of resistance by the FGFR2-fusion+ tumor cells rather than the outgrowth of fusion-negative subclones. A subset of the FGFR2 kinase domain mutations observed in the cfDNA were detected by WES of the post-progression biopsies, whereas none were found in the pre-treatment samples. These secondary mutations included FGFR2 V564F and K659M (Patient #1) and FGFR2 K641R (Patient #2) (Figures 1A and B, *right panels*). Overall, these data are consistent with multiple individual FGFR2 mutations arising in distinct metastatic lesions or in different tumor cells within the same metastatic lesion. These findings also reinforce the inadequacy of single-lesion tumor biopsy to capture the full heterogeneity of resistance mechanisms present in a single patient, and illustrate the potential of cfDNA analysis toward this purpose.

Functional modeling of secondary FGFR2 resistance mutations

All together, six amino acids were affected across the three patients. Notably, structural modeling predicts that each mutation compromises inhibition by BGJ398. The V564F gatekeeper mutation, which was common to all three patients, confers resistance by inducing a steric clash with BGJ398 in its FGFR2 binding pocket (Figure 2A). V564 is in direct contact with the di-chloro, di-methoxy phenyl ring of BGJ398. A residue with a bulkier side chain clashes with this part of the inhibitor. Interestingly, although none of the other five residues are in direct contact with BGJ398, their mutation destabilizes the inactive conformation of the kinase to which BGJ398 binds (Figure 2B). The N549, E565 and K641 triad define a molecular brake that maintains the kinase in an inactive conformation. Thus, mutation of these residues leads to activation of the kinase (21). Mutation of the K659 residue also leads to FGFR2 kinase activation by stabilizing the active conformation of its activation loop (22). Similarly, the effect of the L617 mutation is to weaken a stabilizing interaction of this residue with the phenylalanine residue of the FGFR2 Asp-Phe-Gly (DFG) motif, which normally adopts a special conformation

favoring the binding of inhibitors in the BGJ398 class. Thus, acquired resistance to BGJ398 is associated with the emergence of recurrent and functionally relevant FGFR2 kinase domain mutations in cfDNA.

To model the development of resistance mutations within the FGFR2 kinase domain following exposure to BGJ398, we performed a mutagenesis screen using BaF3 cells engineered to express a TEL-FGFR2 fusion protein. Under growth factor restricted conditions, these cells were dependent on FGFR2 signaling, and were thus sensitive to BGJ398 inhibition. Nevertheless, exposure to lethal doses resulted in the rapid development of resistant cells. Next-generation sequencing of pooled resistant clones identified FGFR2 N549D and V564I mutations at 44.56% and 24.44%, respectively (data not shown), both corresponding to amino acid residues observed in the setting of clinical resistance. Since FGFR2 and FGFR3 share 89% amino acid homology in their kinase domains, all six corresponding residues in FGFR3 would be expected to have the same role in either inducing steric clash with BGJ398 or stabilizing the active kinase conformation (Figure 2C). Accordingly, exposure of TEL-FGFR3 -expressing BaF3 cells to lethal doses of BGJ398 resulted in the rapid formation of resistant colonies harboring five distinct FGFR3 mutations, all of which corresponded to FGFR2 amino acids mutated in Patients #1-3 (Figure 2D). At the lowest dose (100 nM), 10 individual clones were isolated, harboring FGFR3 N540K, V555L, V555M, L608V, and K650E mutations, corresponding to FGFR2 N549, V564, L617, and K659, respectively. By contrast, higher doses of BGJ398 resulted exclusively in colonies harboring the V555M gatekeeper mutation. These mutations decreased the sensitivity of BaF3 cells by 10-1000 fold, with V555M conferring the greatest degree of resistance, consistent with the appearance of the corresponding FGFR2 mutation in all three patients and the predominance of this resistant clone at higher doses of BGJ398 (Figure 2E).

Importantly, the potential for a convergent resistance mechanism involving the FGFR2 kinase domain may have major implications for the selection of subsequent treatment

strategies, as irreversible or structurally distinct FGFR inhibitors have been designed to overcome specific FGFR resistance mutations *in vitro* (23) and are already in clinical trials. Accordingly, we compared the sensitivity of individual resistant clones to a panel of five FGFR inhibitors that are currently in clinical trials, as well as the irreversible inhibitor FIIN-2. Each drug displayed a different profile, with LY2874455 showing the smallest reduction in activity against the different resistance mutations overall, and with ponatinib and dovitinib showing the smallest change against the N540/549K mutation in particular (Figure 2F). Interestingly, LY2874455 and dovitinib rather than FIIN-2, appeared to be least affected by the V555M gatekeeper mutation. Thus, different FGFR inhibitors may have unique abilities to overcome specific secondary mutations arising in cancers with FGFR2 or FGFR3 alterations.

Rapid autopsy reveals inter-tumoral and intra-tumoral heterogeneity of resistance

The identification of five concurrent FGFR2 resistance mutations in the cfDNA of Patients #1 and #2 suggests marked inter- and/or intra-tumoral heterogeneity associated with acquired resistance. Since single-lesion tumor biopsies performed at disease progression exhibited only a subset of these mutations, we performed a rapid autopsy on Patient #2 to obtain a more complete assessment of the genetic alterations present within resistant tumors. This patient passed away 3 months after stopping BGJ398, without any intervening anti-cancer therapies. We collected 10 liver metastases and two lung metastases that were of adequate tumor cellularity for molecular analysis. Quantitative RT-PCR (qRT-PCR) detected the FGFR2-OPTN fusion in all samples, reinforcing the conclusion that resistant tumor cells retain the FGFR2 fusion and that progression is not likely to be driven by the emergence of fusion negative clones (Figure 3A and Supplementary Figure S1A and S1B).

Autopsy specimens along with the original resection specimen and the pre-treatment and post-progression biopsies were analyzed by targeted deep-sequencing using the FoundationOne assay, which assesses the mutational status of 315 cancer-related genes with

>500 fold coverage (Figure 3A). The autopsy specimens exhibited three of the FGFR2 kinase domain mutations that were identified in this patient's post-progression cfDNA (N549H, E565A, and K641R), whereas only K641R was seen in the post-progression tumor biopsy. These mutations were found in four of the 12 distinct metastases analyzed, with one metastasis harboring two concurrent mutations. Despite this extensive analysis of multiple tumor lesions, two FGFR2 mutations identified in cfDNA were still not detected, further demonstrating the significant inter-tumoral heterogeneity of resistant clones.

We next sought to relate the responsiveness of a given lesion to the presence of specific genetic alterations. Spatial correlation of autopsy specimens with the patient's most recent CT scan identified three tumors that were clearly shrinking at the time of progression ('Responsive'), and four tumors were either growing or appeared as new lesions while the patient was receiving BGJ398 ('Resistant') (Figure 3A, *right panel*). Another five tumors appeared following discontinuation of BGJ398 and therefore could not be correlated with clinical response. The characterization of these tumors at the time of autopsy as either clearly 'Resistant' or 'Responsive' was limited by the fact that the autopsy occurred three months after the discontinuation of BGJ398, which may have allowed resistant tumor cells to seed previously responsive tumors or sensitive tumor cells to divide in the absence of selective pressure. Nevertheless, we identified FGFR2 mutations in two of the four 'Resistant' tumors (N549H and K641R) and in two of the five lesions that emerged after discontinuation of BGJ398 (K641R alone or concurrently with E565A), but in none of the "Responsive" lesions. Truncal mutations in PRBM1, ATR, and FBXW7 were observed in all specimens, confirming a common clonal origin. A number of additional mutations were also detected that were specific to different tumors, although their clinical significance remains unclear (Supplementary Figure S2).

Beyond FGFR2 point mutations, several alterations in the PTEN/PI3K pathway were detected, including a PTEN truncation in the post-progression biopsy from Patient #2, resulting from an apparent fusion between *PTEN* and the *COL17A1* locus (Supplementary Figure S3A).

WES analysis revealed single copy loss across the entire long ('q') arm of chromosome 10 including the *PTEN* gene in both pre-treatment and post-progression biopsies from this patient (Supplementary Figure S3B). Thus, the PTEN truncation could represent loss of heterozygosity (LOH) in a subset of tumor cells. Similarly, PTEN nonsense or frameshift mutations were also observed in one responsive lesion and one lesion that emerged after discontinuation of treatment. A single resistant lesion harbored a PIK3CA Q546R mutation, however its significance is uncertain since this mutation was detected in the patient's plasma prior to BGJ398 treatment and decreased in prevalence during therapy (Figure 1B, *left-lower panel*). Thus, it is possible that alteration of the PTEN/PI3K pathway may represent an FGFR2-independent mechanism of resistance to FGFR2 inhibition, although further study is needed.

Finally, we sought to assess the degree of intra-tumoral genomic heterogeneity by conducting multi-region sequencing of two autopsy specimens from Patient #2. One 'Responsive' (Liver Met #1) and one 'Resistant' (Liver Met #2) lesion were each transected into eight individual pieces (Figure 3A, *left-lower panel* and 3B). The responsive Liver Met #1 harbored three distinct PTEN loss-of-function mutations, each found in separate adjacent pieces, suggesting a potential selective advantage of PTEN inactivation in this particular lesion. In the resistant Liver Met #2, the FGFR2 K641R mutation was detected in six of eight tumor pieces, and no other point mutation was observed (Figure 3B). By contrast, multi-region sequencing of the original resection specimen revealed no detectable FGFR2 point mutations or PTEN truncations (Supplementary Figure S4). Taken together, our findings suggest that recurrent secondary FGFR2 kinase domain mutations and molecular heterogeneity confer clinical acquired resistance to FGFR inhibitors in FGFR2-fusion+ ICC, and that therapeutic strategies capable of overcoming this mechanism of resistance may be critical components of future treatments for these cancers.

Discussion

To our knowledge, this study is the first to define mechanisms underlying clinical acquired resistance to FGFR inhibitor therapy. The observation that all three FGFR2-fusion+ ICC patients developed secondary FGFR2 kinase domain mutations, with multiple mutations emerging in two patients, suggests that these alterations are major drivers of clinical resistance to FGFR inhibition. The V564 gatekeeper mutation, which was common to all three patients, and the additional six FGFR2 point mutations identified were predicted to confer resistance by previous *in vitro* studies and structural modeling (21-25). These findings may have more general significance since equivalent FGFR2 point mutations exist *de novo* in many cancers (25). Moreover, FGFR3 fusions are present in several malignancies, including glioblastoma multiforme, bladder cancer, and lung adenocarcinoma (26), and our *in vitro* data suggest that mutations in corresponding amino acids in FGFR3 may cause resistance to FGFR inhibitors in this context. Importantly, the discoveries reported here have immediate clinical implications since covalent FGFR inhibitors designed to overcome such mutations have recently been developed, including TAS-120, an irreversible FGFR inhibitor that has already entered phase I testing (NCT02052778) (27).

The rapid acquisition of heterogeneous resistance mutations can undoubtedly create challenges for the establishment of more effective therapeutic strategies. However, prior studies have illustrated that similar convergent evolution of resistance through multiple secondary kinase mutations in ALK fusion-positive non-small cell lung cancers can be overcome clinically by structurally optimized inhibitors (28), suggesting a similar strategy may be effective in this scenario. Notable in this regard, we found that a collection of structurally and functionally distinct clinical and preclinical FGFR inhibitors displayed varying abilities to overcome specific resistance mutations. LY2874455, for instance, appeared to be the compound least affected by the panel of resistance mutations, but still showed reduced activity in the N540/549K mutated model (Figure 2F). Conversely, ponatinib activity was not affected by this mutation, but showed

markedly decreased efficacy in the setting of the gatekeeper mutation. Thus, our study highlights the potential limitations of any single compound and suggests that future development of FGFR inhibitors should focus on agents capable of surmounting multiple common secondary resistance mutations.

It is also possible that FGFR2-independent mechanisms may contribute to acquired resistance and further limit the efficacy of next-generation FGFR inhibitors. In our study, patient #2 had a PTEN loss of function mutation in the biopsy tissue of a lesion that was clearly progressing on BGJ398 and had additional PI3K/PTEN pathway mutations in four of twelve metastases analyzed at rapid autopsy (Figure 3A). It is notable that three distinct inactivating PTEN mutations were detected in the residual tissue from a single “Responsive” tumor, suggesting there was a significant selective advantage granted by PTEN LOH in this lesion. Interestingly, knockdown of PTEN was recently found to confer resistance to loss of FGFR2 signaling in FGFR2-amplified cell lines (29). The PI3KCA Q546R mutation, however, was detectable in patient #2’s cfDNA prior to initiation of therapy (Figure 1B, left-lower panel), and levels of this mutation tracked with those of a truncal PBRM1 nonsense mutation, implying that this mutation did not emerge during therapy. Thus, future studies will be needed to determine whether activation of the PI3K/PTEN pathway serves as an FGFR-independent resistance mechanism in FGFR-driven cancers.

Our findings also highlight the potential advantages of cfDNA analysis in the monitoring and clinical management of patients undergoing FGFR inhibitor therapy. While cfDNA analysis detected multiple distinct resistant clones emerging concurrently in different tumors within the same patient, a single post-progression biopsy, or even extensive tumor sampling at rapid autopsy, was unable to identify the full spectrum of resistance mutations detected in the plasma of these patients. cfDNA, which may reflect DNA shed from multiple metastatic sites, can thus offer a non-invasive and efficient approach to capturing intra- and inter-tumoral heterogeneity in the setting of resistance (30). Furthermore, since structurally distinct FGFR inhibitors display

varying abilities to overcome different secondary FGFR2 resistance mutations, real-time detection and monitoring of clonal evolution of individual mutations may be a valuable tool to guide the selection of the appropriate inhibitors for patient management. Thus, a combined approach integrating cfDNA analysis with direct tumor sampling may represent an important approach to guide clinical decision-making.

Overall, these studies indicate that recurrent secondary FGFR2 kinase domain mutations are a common mechanism of clinical resistance to FGFR inhibition. Importantly, our data also suggest that resistant clones harboring such mutations are likely to retain dependence on FGFR2 signaling, implying that structural optimization of next-generation FGFR inhibitors is needed to promote more durable remissions in FGFR2-fusion+ ICC and other cancers harboring alterations in the FGFR signaling pathway.

Methods

Patients. Patients provided written informed consent to treatment on the phase II trial of BGJ398 (NCT02160041) at the Massachusetts General Hospital (MGH) Cancer Center. They received a 100mg capsule and a 25mg capsule of BGJ398 daily for days 1-21 of each 28 day cycle, and all dose reductions and safety assessments were performed per protocol. Computed tomography and/or magnetic resonance imaging scans were performed at baseline and every 8 weeks to assess for tumor response by RECIST version 1.1 criteria. All biopsies, tumor specimens, and peripheral blood draws for plasma isolation were collected and analyzed in accordance with Institutional Review Board-approved protocols, to which patients provided written informed consent, and all studies were conducted in accordance with the Declaration of Helsinki. Rapid autopsy on patient #1 was performed within the first three hours *post mortem*.

Solid Fusion Assay (SFA). Our internal tumor profiling assay was performed on RNA extracted

from formalin-fixed paraffin-embedded (FFPE) specimens as part of routine clinical care. The SFA is a targeted RNA sequencing method of Anchored Multiplex PCR (AMP) to detect FGFR2 fusions, and the methodology has been previously described (19). Mutational profiling was performed at the Clinical Laboratory Improvement Amendments–certified Translational Research Laboratory at the Massachusetts General Hospital Cancer Center.

Targeted Sequencing of Tumor Tissue. DNA derived from the primary tumor, serial biopsies of liver metastases, autopsy specimens from liver and lung metastases, and matched normal muscle tissue were analyzed using deep-coverage targeted sequencing of key cancer-associated genes. Tumor samples sent for analysis had $\geq$ 10% tumor cellularity as determined by review of a hematoxylin and eosin slide by a board certified pathologist (V.D.). Targeted sequencing was performed via the FoundationOne platform, version T5, and the methodology has been previously described (31).

Quantitative Polymerase Chain Reaction on Tumor Tissue for Detection of the FGFR-OPTN Fusion on Autopsy Samples. Autopsy specimens of Patient #1 were homogenized with a tissue homogenizer and total RNA was extracted using the RNeasy Mini Kit (Qiagen) according to the manufacturer's recommended protocol. cDNA synthesis was performed using the QuantiTect Reverse Transcription Kit (Qiagen) with 1 ug total RNA. All qPCR reactions were performed using the iTaq Universal SYBR Green Supermix (Bio-Rad) and CFX384 Touch Real-Time PCR Detection System (Bio-Rad). The following primers were used to detect the *FGFR2-OPTN* fusion breakpoint: 5'-TGATGATGAGGGACTGTTGG-3' and 5'-GCCCAGGACTATGCTTGATT-3'. Relative expression levels of the fusion protein were normalized to expression of *RNA18S5*: 5'- CGTCTGCCCTATCAACTTTCG-3' and 5'-TGCCTTCCTTGGATGTGGTAG-3'.

Plasma cfDNA isolation and quantification of genome equivalents. At least 10 mL of whole blood were collected by blood draw using EDTA as anticoagulant. Plasma was separated within 5 hours through 2 different centrifugation steps (the first at room temperature for 10 minutes at 1,600 × g and the second at 3,000 × g for the same time and temperature), obtaining up to 3 mL of plasma. Plasma was stored at -80°C until cfDNA extraction. cfDNA was extracted from plasma using the QIAamp Circulating Nucleic Acid Kit (QIAGEN) according to the manufacturer's instructions. 6 µl of cfDNA were used as template for each reaction. All samples were analyzed in triplicate. PCR reactions were performed using 10 µl final volume containing 5 µl GoTaq® qPCR Master Mix, 2X with CXR Reference Dye) (Promega) and LINE-1 [12,5 µmol] forward and reverse primers. DNA at known concentrations was also used to build the standard curve. Primer sequences are available upon request.

Droplet digital PCR. 8 to 10 µl of DNA template was added to 10 µl of ddPCR™ Supermix for Probes (Bio-Rad) and 2 µl of the primer/probe mixture. This reaction mix was added to a DG8 cartridge together with 60µl of Droplet Generation Oil for Probes (Bio-Rad) and used for droplet generation. Droplets were then transferred to a 96 well plate (Eppendorf) and then thermal cycled with the following conditions: 5 minutes at 95°C, 40 cycles of 94°C for 30s, 55°C for 1 minute followed by 98°C for 10 minutes (Ramp Rate 2°C/sec). Droplets were analyzed with the QX200™ Droplet Reader (Bio-Rad) for fluorescent measurement of FAM and HEX probes. Gating was performed based on positive and negative controls, and mutant populations were identified. The ddPCR data were analyzed with QuantaSoft analysis software (Bio-Rad) to obtain Fractional Abundance of the mutant DNA alleles in the wild-type/normal background. The quantification of the target molecule was presented as number of total copies (mutant plus WT) per sample in each reaction. Fractional Abundance is calculated as follows: F.A. % = (Nmut/(Nmut+Nwt))*100), where Nmut is number of mutant events and Nwt is number of WT

events per reaction. ddPCR analysis of normal control plasma DNA (from cell lines) and no DNA template controls were always included. Probe and primer sequences are available upon request.

In vitro studies on FGFR-driven BaF3 cells. BaF3 TEL-FGFR2 or BaF3 TEL-FGFR3 cells were mutagenized with the alkylating agent N-ethyl-N-nitrosourea, and resistant clones were selected in presence of different concentrations of BGJ398 as previously described (32). In brief, mutagenized cells were distributed into 96-well plates with 100 / 200 / 400 / 800 / 1600 nM BGJ398 (3 plates each), placing 10^5 cells in 100 μL media into each well. Outgrowing clones were picked and expanded during days 13 to 24 with the original concentration of BGJ398. Mutations in the FGFR3 kinase domain were determined by PCR and Sanger sequencing. Sequencing traces suggested that pure clones with single point mutations were obtained in all cases.

For proliferation assays with various FGFR inhibitors, For proliferation assays, BaF3 cells were seeded on 96-well-plates in triplicates at 10000 cells per well and incubated with various concentrations of FGFR inhibitors for 72 hours followed by quantification of viable cells using a resazurin sodium salt dye reduction readout (commercially known as AlamarBlue assay). IC50 values were determined with the XLFit Excel Add-In (ID Business Solutions) using a 4-parameter dose response model. BGJ398 was synthesized at Novartis and other FGFR inhibitors were obtained from commercial sources.

Homology Models of FGFR2 and FGFR3 in complex with BGJ398. The sequences of the human FGFR2 and FGFR3 kinases were obtained from SWISS-PROT (33), entries P21802 and P22607, respectively. The crystallographic structure of the FGFR1 kinase in complex with the inhibitor BGJ398 (PDB code 3TT0 from the Protein Data Bank) was chosen as template. The sequences were aligned using T-Coffe (34). On the basis of the resulting alignment, the 3D

structures of the FGFR2 and FGFR3 kinases were modeled using the What If program (35) with the default parameters (PIRPSQ module, BLDPIR command). The figures for the structural models were prepared using PYMOL (Schrodinger, Inc.).

Whole-exome sequencing and RNA sequencing. Whole-exome and RNA sequencing was performed by the Broad Institute sequencing platform. Whole-exome sequencing of matched pre-treatment and post-progression biopsies and normal blood was performed as previously described (36). All BAM files will be deposit in dbGAP prior to publication. Detailed methods for RNA sequencing are as follows. RNA was extracted from patient tumor biopsies using the AllPrep DNA/RNA kit (Qiagen) according to the manufacturer's instructions. All samples were quantified using Nanodrop and quality was evaluated using Agilent's Bioanalyzer 2100.

RNA samples and two positive controls (K-562) were assessed for quality using Agilent's Bioanalyzer 2100. The percentage of fragments with a size greater than 200 nucleotides (DV_{200}) was calculated using the Agilent software. Samples with a DV_{200} score less than 30% were not included, as the likelihood of success is dramatically reduced with these more fragmented samples (see Illumina technote: http://www.illumina.com/documents/products/technotes/technote-truseq-rna-access.pdf).

100ng of RNA was used as the input for first strand cDNA synthesis using Superscript III reverse transcriptase (Life Technologies, Cat. #18080044) and Illumina's TruSeq Stranded Total RNA Sample Prep Kit (Illumina, Cat. #RS-122-2201). The fragmentation step prior to cDNA synthesis was omitted in the FFPE RNA samples, only the K-562 positive control samples were fragmented at 94°C for 8 minutes. Synthesis of the second strand of cDNA was followed by indexed adapter ligation. Subsequent PCR amplification enriched for adapted fragments. The amplified libraries were quantified using a Qubit assay (Life Technologies, Cat. #Q3285) and assessed for quality on an Agilent Technologies 2100 Bioanalyzer (DNA 1000 chip).

200ng of each cDNA library, not including controls, were combined into two 4-plex pools. Illumina's Coding Exome Oligos (Illumina, Part #15034575) that target the exome were added, and hybridized on a thermacycler with the following conditions: 95°C for 10 minutes, 18 cycles of 1 minute incubations starting at 94°C, then decreasing 2°C per cycle, then 58°C for 90 minutes. Following hybridization, streptavidin beads were used to capture the probes that were hybridized in the previous step. Two wash steps effectively remove any non-specifically bound products. These same hybridization, capture and wash steps are repeated to assure high specificity.

A second round of amplification enriches the captured libraries. qPCR (Kapa Biosystems, Cat. #KK4600) was performed on the pooled libraries and normalized to 2nM. The normalized, pooled libraries were loaded onto HiSeq2500 for a target of 50 million 2x76bp paired reads per sample.

Acknowledgements

The authors acknowledge Guardant Health, Richard Lanman, and Rebecca Nagy for assistance with cfDNA analysis with the Guardant360 assay.

Figure Legends

Figure 1. Clinical acquired resistance to BGJ398.

A-C. *Left-upper panels*. Graphs illustrating serial CA19-9 serum levels and tumor volume measurements by RECISTv1.1 criteria for Patients 1-3, respectively. The pink box indicates time while the patient was receiving BGJ398. *Right panels*, CT scans demonstrating initial response lesions that subsequently progressed despite BGJ398 therapy. Inset shows higher

magnification of responsive/resistant lesion. FGFR2-related genetic events detected by Solid Fusion Assay (SFA), RNA sequencing, whole-exome sequencing (WES), or the Guardant360 assay are documented in the text below CT images. *Left-lower panels*, Percent allele burden in cfDNA of the indicated mutations from Patient #1 (**A**) and Patient #2 (**B**) and Patient #3 (**C**) were monitored over time. The pink box indicates time while the patient was receiving BGJ398. N.D. = not detected.

Figure 2. FGFR point mutations confer resistance to BGJ398 and other FGFR inhibitors.

A. *In silico* model of BGJ398 in binding pocket of FGFR2, demonstrating steric clash in the context of a V564F mutation.

B and C. Model of wild-type FGFR2 (**A**) and FGFR3 (**B**) bound to BGJ398 with relevant amino acids highlighted and color-coded.

D. BaF3 cells were engineered to express a TEL-FGFR3 fusion protein and subjected to a mutagenesis screen at increasing doses of BGJ398. The bar graph indicates the number of BGJ398-resistant clones isolated with indicated FGFR3 point mutations. Corresponding FGFR2 amino acids are indicated after the '/'. Overall, the estimated frequency of cells that acquired a resistance mutation during the screen was approximately 1 in 5 million.

E. BaF3 cells engineered to express wild-type (WT) TEL-FGFR3 fusion or individual clones from the mutagenesis screen bearing the indicated mutants and treated with increasing doses of BGJ398 and proliferation was quantified after 3 days with Alamar blue.

F. IC50 values for BaF3 cells expressing the indicated constructs and treated with the indicated FGFR inhibitor.

Figure 3. Rapid autopsy reveals inter-tumoral and intra-tumoral heterogeneity of resistance.

A. *Left-upper panel*, Corresponding images of four liver mets taken from Patient #2's most recent CT scan (top) and autopsy (bottom). *Right-upper panel*, Heatmap illustrating mutations detected in the indicated autopsy lesions. Four distinct PTEN mutations and three distinct FGFR2 point mutations were identified. *Left-lower panel*, Heatmap indicating mutations identified in eight spatially distinct pieces isolated from Liver Met#1.

B. *Left panels*, Corresponding images of Liver Met #2 taken from Patient #2's most recent CT scan (left) and autopsy (right). *Right panel*, Heatmap indicating mutations detected in eight spatially distinct pieces from Liver Met #2.

Supplementary Figure S1. FGFR2-OPTN fusion detected in all autopsy lesions.

A. Relative expression of the FGFR2-OPTN fusion in the indicated autopsy lesions as measured by real-time quantitative PCR (RT-qPCR).

B. PCR product isolated from **A**, in the presence or absence of reverse transcriptase (RT), was resolved on an agarose gel.

Supplementary Figure S2. FoundationOne analysis of autopsy lesions

Heatmap indicating all genetic events identified in the indicated Patient #2 lesions. Gray boxes indicate mutations of undetermined significance.

Supplementary Figure S3. *PTEN* loss of heterozygosity (LOH) identified in Patient #2.

A. Intrachromosomal fusion event detected by FoundationOne assay in the post-progression biopsy sample from patient #2 and leading to *PTEN* LOH.

B. Heatmap illustrating the relative copy number along chromosome 10 in normal tissue, pre-treatment and post-progression biopsies from Patient #1 and Patient #2 as determined by WES. Note: Patient #2 demonstrates loss of the entire long arm of chromosome 10q as an early event (pre-treatment).

Supplementary Figure S4. Mutational analysis of original resection specimen from Patient #2. *Top panel*, CT image of resected lesion from Patient #2. *Bottom panel*, Heatmap illustrating detected mutations in six spatially distinct pieces isolated from the resection specimen by FoundationOne assay.

References

1. Turner N, Grose R. Fibroblast growth factor signalling: from development to cancer. Nat Rev Cancer. 2010;10:116-29.
2. Hallinan N, Finn S, Cuffe S, Rafee S, O'Byrne K, Gately K. Targeting the fibroblast growth factor receptor family in cancer. Cancer treatment reviews. 2016;46:51-62.
3. Saha SK, Zhu AX, Fuchs CS, Brooks GA. Forty-Year Trends in Cholangiocarcinoma Incidence in the U.S.: Intrahepatic Disease on the Rise. The oncologist. 2016;21:594-9.
4. Shaib Y, El-Serag HB. The epidemiology of cholangiocarcinoma. Seminars in liver disease. 2004;24:115-25.
5. Valle J, Wasan H, Palmer DH, Cunningham D, Anthoney A, Maraveyas A, et al. Cisplatin plus gemcitabine versus gemcitabine for biliary tract cancer. N Engl J Med. 2010;362:1273-81.
6. Arai Y, Totoki Y, Hosoda F, Shirota T, Hama N, Nakamura H, et al. Fibroblast growth factor receptor 2 tyrosine kinase fusions define a unique molecular subtype of cholangiocarcinoma. Hepatology. 2014;59:1427-34.
7. Graham RP, Barr Fritcher EG, Pestova E, Schulz J, Sitailo LA, Vasmatzis G, et al. Fibroblast growth factor receptor 2 translocations in intrahepatic cholangiocarcinoma. Human pathology. 2014;45:1630-8.
8. Ross JS, Wang K, Gay L, Al-Rohil R, Rand JV, Jones DM, et al. New routes to targeted therapy of intrahepatic cholangiocarcinomas revealed by next-generation sequencing. The oncologist. 2014;19:235-42.
9. Sia D, Losic B, Moeini A, Cabellos L, Hao K, Revill K, et al. Massive parallel sequencing uncovers actionable FGFR2-PPHLN1 fusion and ARAF mutations in intrahepatic cholangiocarcinoma. Nature communications. 2015;6:6087.
10. Voss JS, Holtegaard LM, Kerr SE, Fritcher EG, Roberts LR, Gores GJ, et al. Molecular profiling of cholangiocarcinoma shows potential for targeted therapy treatment decisions. Human pathology. 2013;44:1216-22.
11. Wu YM, Su F, Kalyana-Sundaram S, Khazanov N, Ateeq B, Cao X, et al. Identification of targetable FGFR gene fusions in diverse cancers. Cancer discovery. 2013;3:636-47.
12. Borad MJ, Champion MD, Egan JB, Liang WS, Fonseca R, Bryce AH, et al. Integrated genomic characterization reveals novel, therapeutically relevant drug targets in FGFR and EGFR pathways in sporadic intrahepatic cholangiocarcinoma. PLoS genetics. 2014;10:e1004135.
13. Wang Y, Ding X, Wang S, Moser CD, Shaleh HM, Mohamed EA, et al. Antitumor effect of FGFR inhibitors on a novel cholangiocarcinoma patient derived xenograft mouse model endogenously expressing an FGFR2-CCDC6 fusion protein. Cancer Letters. 2016;380:163-73.
14. Guagnano V, Furet P, Spanka C, Bordas V, Le Douget M, Stamm C, et al. Discovery of 3-(2,6-dichloro-3,5-dimethoxy-phenyl)-1-{6-[4-(4-ethyl-piperazin-1-yl)-phenylamino]-pyrimidin-4-yl}-1-methyl-

urea (NVP-BGJ398), a potent and selective inhibitor of the fibroblast growth factor receptor family of receptor tyrosine kinase. Journal of medicinal chemistry. 2011;54:7066-83.
15. Guagnano V, Kauffmann A, Wöhrle S, Stamm C, Ito M, Barys L, et al. FGFR genetic alterations predict for sensitivity to NVP-BGJ398, a selective pan-FGFR inhibitor. Cancer discovery. 2012;2:1118-33.
16. Javle MM, Shroff RT, Zhu AX, Sadeghi S, Choo S, Borad MJ, et al. A phase 2 study of BGJ398 in patients (pts) with advanced or metastatic FGFR-altered cholangiocarcinoma (CCA) who failed or are intolerant to platinum-based chemotherapy. Gastrointestinal Cancers Symposium. San Francisco, CA: J Clin Oncol 34, 2016 (suppl 4S; abstr 335); 2015.
17. Garraway LA, Janne PA. Circumventing cancer drug resistance in the era of personalized medicine. Cancer discovery. 2012;2:214-26.
18. Holohan C, Van Schaeybroeck S, Longley DB, Johnston PG. Cancer drug resistance: an evolving paradigm. Nature reviews Cancer. 2013;13:714-26.
19. Zheng Z, Liebers M, Zhelyazkova B, Cao Y, Panditi D, Lynch KD, et al. Anchored multiplex PCR for targeted next-generation sequencing. Nature medicine. 2014;20:1479-84.
20. Kim ST, Lee WS, Lanman RB, Mortimer S, Zill OA, Kim KM, et al. Prospective blinded study of somatic mutation detection in cell-free DNA utilizing a targeted 54-gene next generation sequencing panel in metastatic solid tumor patients. Oncotarget. 2015;6:40360-9.
21. Chen H, Ma J, Li W, Eliseenkova AV, Xu C, Neubert TA, et al. A molecular brake in the kinase hinge region regulates the activity of receptor tyrosine kinases. Molecular cell. 2007;27:717-30.
22. Huang Z, Chen H, Blais S, Neubert TA, Li X, Mohammadi M. Structural mimicry of a-loop tyrosine phosphorylation by a pathogenic FGF receptor 3 mutation. Structure. 2013;21:1889-96.
23. Tan L, Wang J, Tanizaki J, Huang Z, Aref AR, Rusan M, et al. Development of covalent inhibitors that can overcome resistance to first-generation FGFR kinase inhibitors. Proceedings of the National Academy of Sciences of the United States of America. 2014;111:E4869-77.
24. Byron SA, Chen H, Wortmann A, Loch D, Gartside MG, Dehkhoda F, et al. The N550K/H mutations in FGFR2 confer differential resistance to PD173074, dovitinib, and ponatinib ATP-competitive inhibitors. Neoplasia. 2013;15:975-88.
25. Patani H, Bunney TD, Thiyagarajan N, Norman RA, Ogg D, Breed J, et al. Landscape of activating cancer mutations in FGFR kinases and their differential responses to inhibitors in clinical use. Oncotarget. 2016;7:24252-68.
26. Stransky N, Cerami E, Schalm S, Kim JL, Lengauer C. The landscape of kinase fusions in cancer. Nature communications. 2014;5:4846.
27. Ochiiwa H, Fujita H, Itoh K, Sootome H, Hashimoto A, Fujioka Y, et al. Abstract A270: TAS-120, a highly potent and selective irreversible FGFR inhibitor, is effective in tumors harboring various FGFR gene abnormalities. American Association for Cancer Research. 2013;12:A270-A.
28. Gainor JF, Dardaei L, Yoda S, Friboulet L, Leshchiner I, Katayama R, et al. Molecular Mechanisms of Resistance to First- and Second-Generation ALK Inhibitors in ALK-Rearranged Lung Cancer. Cancer discovery. 2016.
29. Pearson A, Smyth E, Babina IS, Herrera-Abreu MT, Tarazona N, Peckitt C, et al. High-Level Clonal FGFR Amplification and Response to FGFR Inhibition in a Translational Clinical Trial. Cancer discovery. 2016;6:838-51.
30. Russo M, Siravegna G, Blaszkowsky LS, Corti G, Crisafulli G, Ahronian LG, et al. Tumor Heterogeneity and Lesion-Specific Response to Targeted Therapy in Colorectal Cancer. Cancer discovery. 2016;6:147-53.
31. Frampton GM, Fichtenholtz A, Otto GA, Wang K, Downing SR, He J, et al. Development and validation of a clinical cancer genomic profiling test based on massively parallel DNA sequencing. Nat Biotechnol. 2013;31:1023-31.

32. Tiedt R, Degenkolbe E, Furet P, Appleton BA, Wagner S, Schoepfer J, et al. A drug resistance screen using a selective MET inhibitor reveals a spectrum of mutations that partially overlap with activating mutations found in cancer patients. Cancer research. 2011;71:5255-64.
33. Bairoch A, Boeckmann B. The SWISS-PROT protein sequence data bank: current status. Nucleic acids research. 1994;22:3578-80.
34. Notredame C, Higgins DG, Heringa J. T-Coffee: A novel method for fast and accurate multiple sequence alignment. Journal of molecular biology. 2000;302:205-17.
35. Vriend G. WHAT IF: a molecular modeling and drug design program. Journal of molecular graphics. 1990;8:52-6, 29.
36. Ahronian LG, Sennott EM, Van Allen EM, Wagle N, Kwak EL, Faris JE, et al. Clinical Acquired Resistance to RAF Inhibitor Combinations in BRAF-Mutant Colorectal Cancer through MAPK Pathway Alterations. Cancer discovery. 2015;5:358-67.

Figure 1

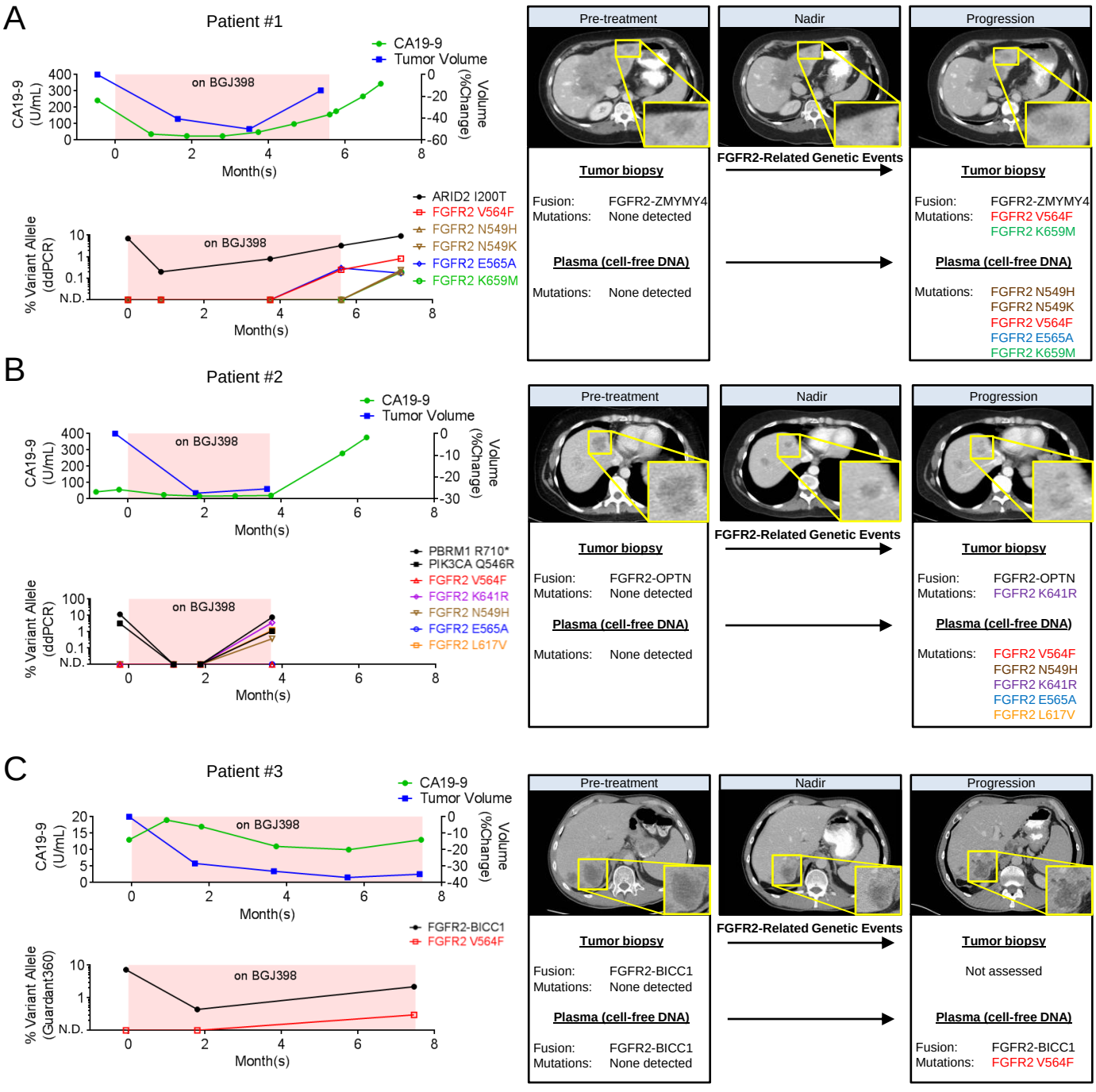
A
Patient #1
CA19-9
Tumor Volume
CA19-9 (U/mL)
Volume (%Change)
on BGJ398
Month(s)
% Variant Allele (ddPCR)
ARID2 I200T
FGFR2 V564F
FGFR2 N549H
FGFR2 N549K
FGFR2 E565A
FGFR2 K659M
N.D.
Pre-treatment
Nadir
Progression
Tumor biopsy
Fusion: FGFR2-ZMYMY4
Mutations: None detected
Plasma (cell-free DNA)
Mutations: None detected
FGFR2-Related Genetic Events
Tumor biopsy
Fusion: FGFR2-ZMYMY4
Mutations: FGFR2 V564F
FGFR2 K659M
Plasma (cell-free DNA)
Mutations: FGFR2 N549H
FGFR2 N549K
FGFR2 V564F
FGFR2 E565A
FGFR2 K659M
B
Patient #2
CA19-9
Tumor Volume
on BGJ398
Month(s)
% Variant Allele (ddPCR)
PBRM1 R710*
PIK3CA Q546R
FGFR2 V564F
FGFR2 K641R
FGFR2 N549H
FGFR2 E565A
FGFR2 L617V
N.D.
Pre-treatment
Nadir
Progression
Tumor biopsy
Fusion: FGFR2-OPTN
Mutations: None detected
Plasma (cell-free DNA)
Mutations: None detected
FGFR2-Related Genetic Events
Tumor biopsy
Fusion: FGFR2-OPTN
Mutations: FGFR2 K641R
Plasma (cell-free DNA)
Mutations: FGFR2 V564F
FGFR2 N549H
FGFR2 K641R
FGFR2 E565A
FGFR2 L617V
C
Patient #3
CA19-9
Tumor Volume
on BGJ398
Month(s)
% Variant Allele (Guardant360)
FGFR2-BICC1
FGFR2 V564F
N.D.
Pre-treatment
Nadir
Progression
Tumor biopsy
Fusion: FGFR2-BICC1
Mutations: None detected
Plasma (cell-free DNA)
Fusion: FGFR2-BICC1
Mutations: None detected
FGFR2-Related Genetic Events
Tumor biopsy
Not assessed
Plasma (cell-free DNA)
Fusion: FGFR2-BICC1
Mutations: FGFR2 V564F

Figure 2

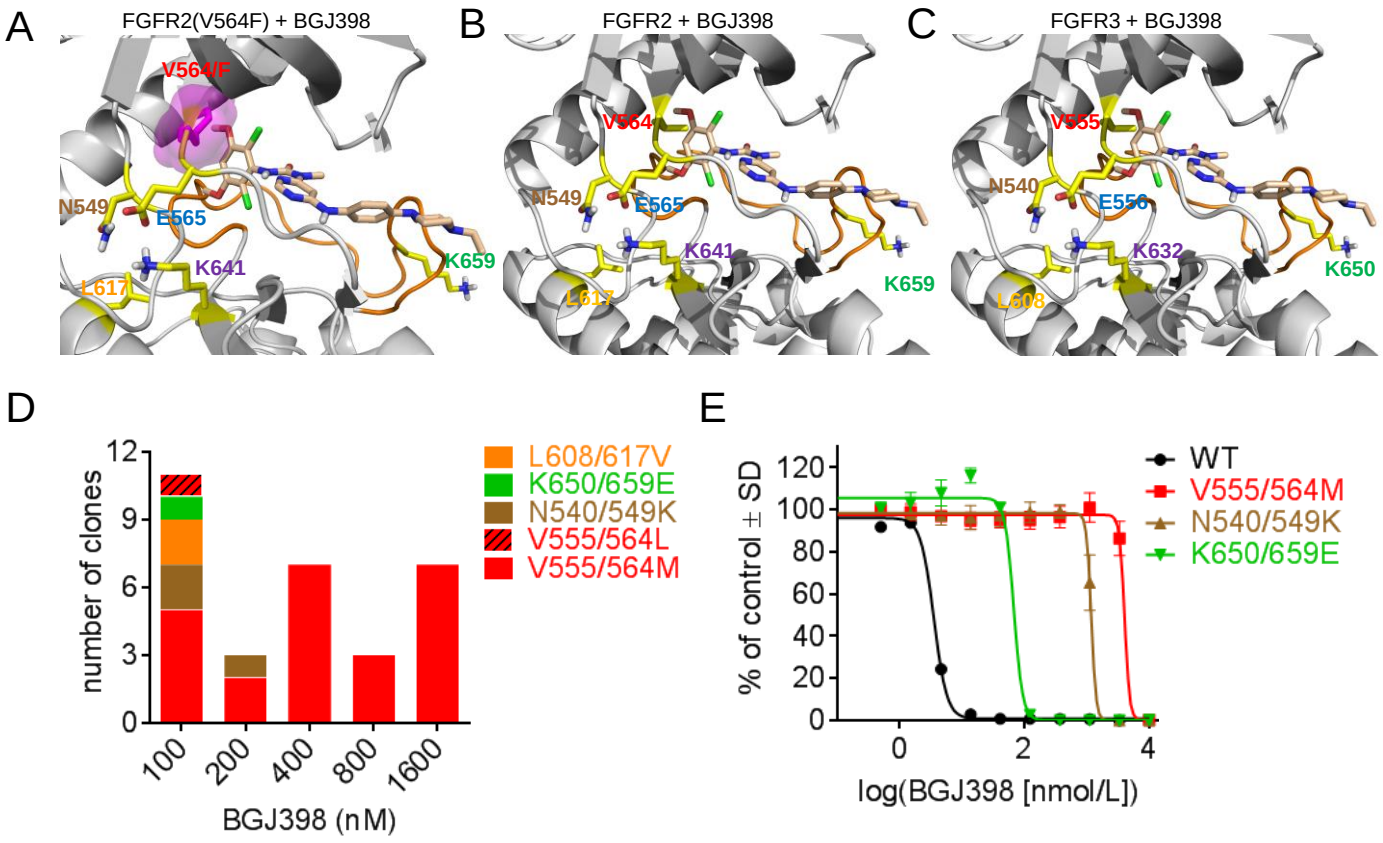

F

	BGJ398		Ponatinib		Dovitinib		AZD-4547		Debio-1347		FIIN-2		LY2874455	
	IC50 (nM)	foldΔ	IC50 (nM)	foldΔ	IC50 (nM)	foldΔ	IC50 (nM)	foldΔ	IC50 (nM)	foldΔ	IC50 (nM)	foldΔ	IC50 (nM)	foldΔ
BaF3	4156	1129	>10000	>15	1453	33	8493	969	>10000	>190	>1000	>2300	66	874
TEL-FGFR3	4	1	650	1	44	1	9	1	52	1	0.43	1	0.08	1
TEL-FGFR3(L608V)	138	38	4259	7	653	15	463	53	2389	46	5	12	0.51	7
TEL-FGFR3(V555M)	1491	405	>10000	>15	148	3	1810	207	8383	163	62	143	0.30	4
TEL-FGFR3(N540K)	433	118	814	1	1049	24	3162	361	4360	85	43	100	3	44
TEL-FGFR3(K650E)	32	9	7507	12	784	18	204	23	1265	25	4	10	0.71	9

Figure 3

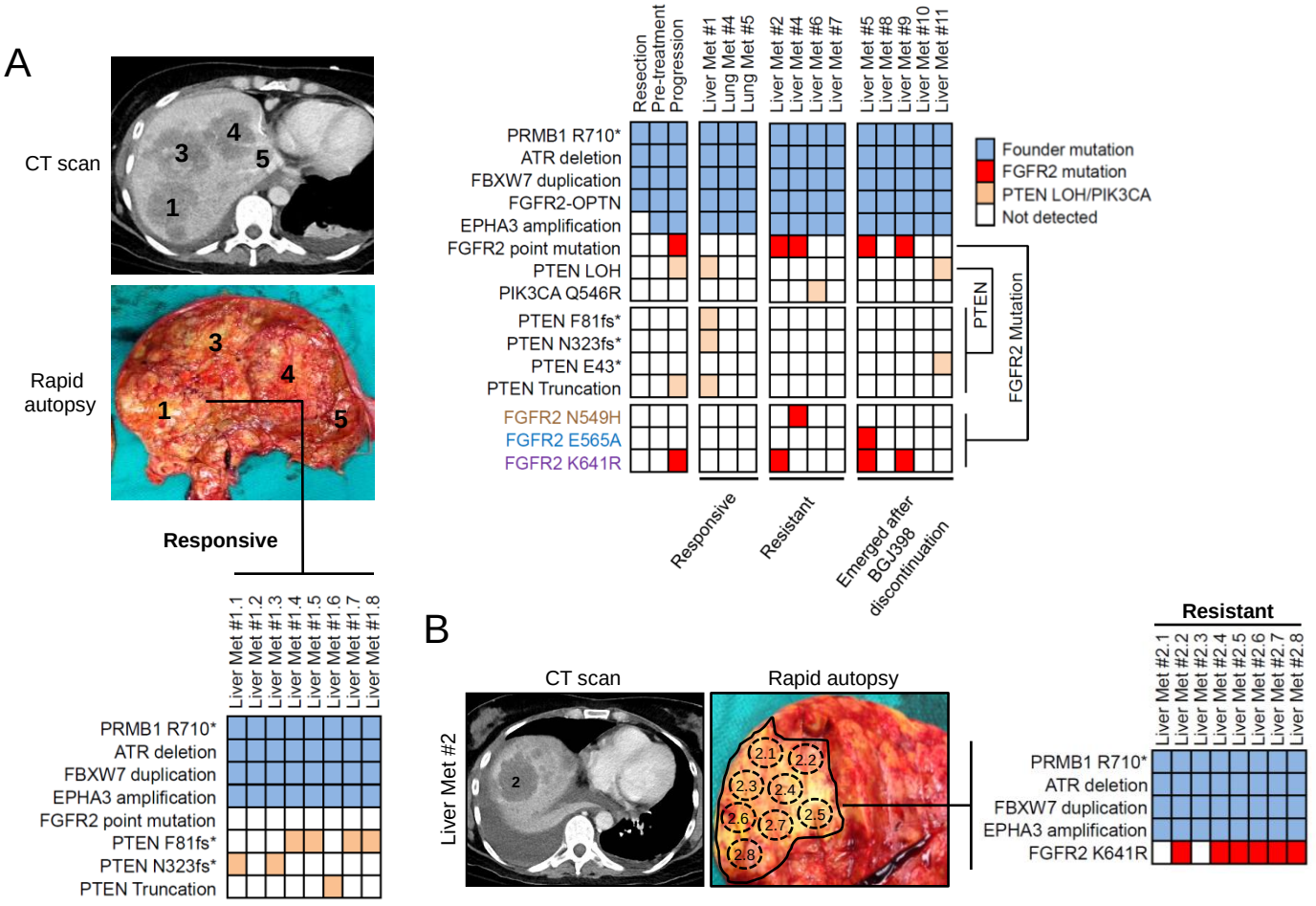
A
CT scan
Rapid autopsy
1
3
4
5
Responsive
Liver Met #1.1
Liver Met #1.2
Liver Met #1.3
Liver Met #1.4
Liver Met #1.5
Liver Met #1.6
Liver Met #1.7
Liver Met #1.8
PRMB1 R710*
ATR deletion
FBXW7 duplication
EPHA3 amplification
FGFR2 point mutation
PTEN F81fs*
PTEN N323fs*
PTEN Truncation
Resection
Pre-treatment
Progression
Liver Met #1
Lung Met #4
Lung Met #5
Liver Met #2
Liver Met #4
Liver Met #6
Liver Met #7
Liver Met #5
Liver Met #8
Liver Met #9
Liver Met #10
Liver Met #11
PRMB1 R710*
ATR deletion
FBXW7 duplication
FGFR2-OPTN
EPHA3 amplification
FGFR2 point mutation
PTEN LOH
PIK3CA Q546R
PTEN F81fs*
PTEN N323fs*
PTEN E43*
PTEN Truncation
FGFR2 N549H
FGFR2 E565A
FGFR2 K641R
Founder mutation
FGFR2 mutation
PTEN LOH/PIK3CA
Not detected
PTEN
FGFR2 Mutation
Responsive
Resistant
Emerged after BGJ398 discontinuation
B
CT scan
Rapid autopsy
Liver Met #2
2
2.1
2.2
2.3
2.4
2.5
2.6
2.7
2.8
Resistant
Liver Met #2.1
Liver Met #2.2
Liver Met #2.3
Liver Met #2.4
Liver Met #2.5
Liver Met #2.6
Liver Met #2.7
Liver Met #2.8
PRMB1 R710*
ATR deletion
FBXW7 duplication
EPHA3 amplification
FGFR2 K641R

Supplementary Figure S1

A

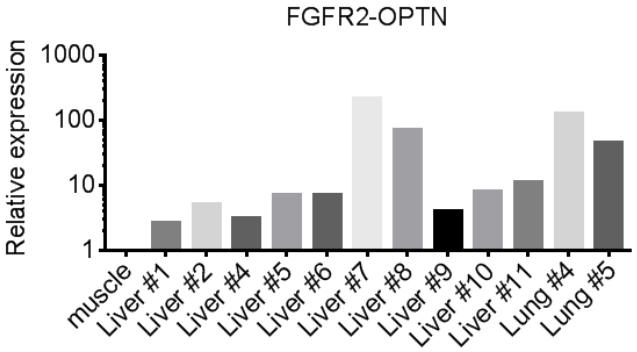

B

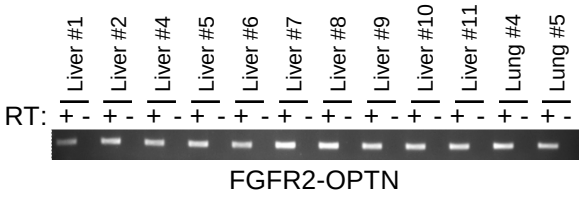

Supplementary Figure S2

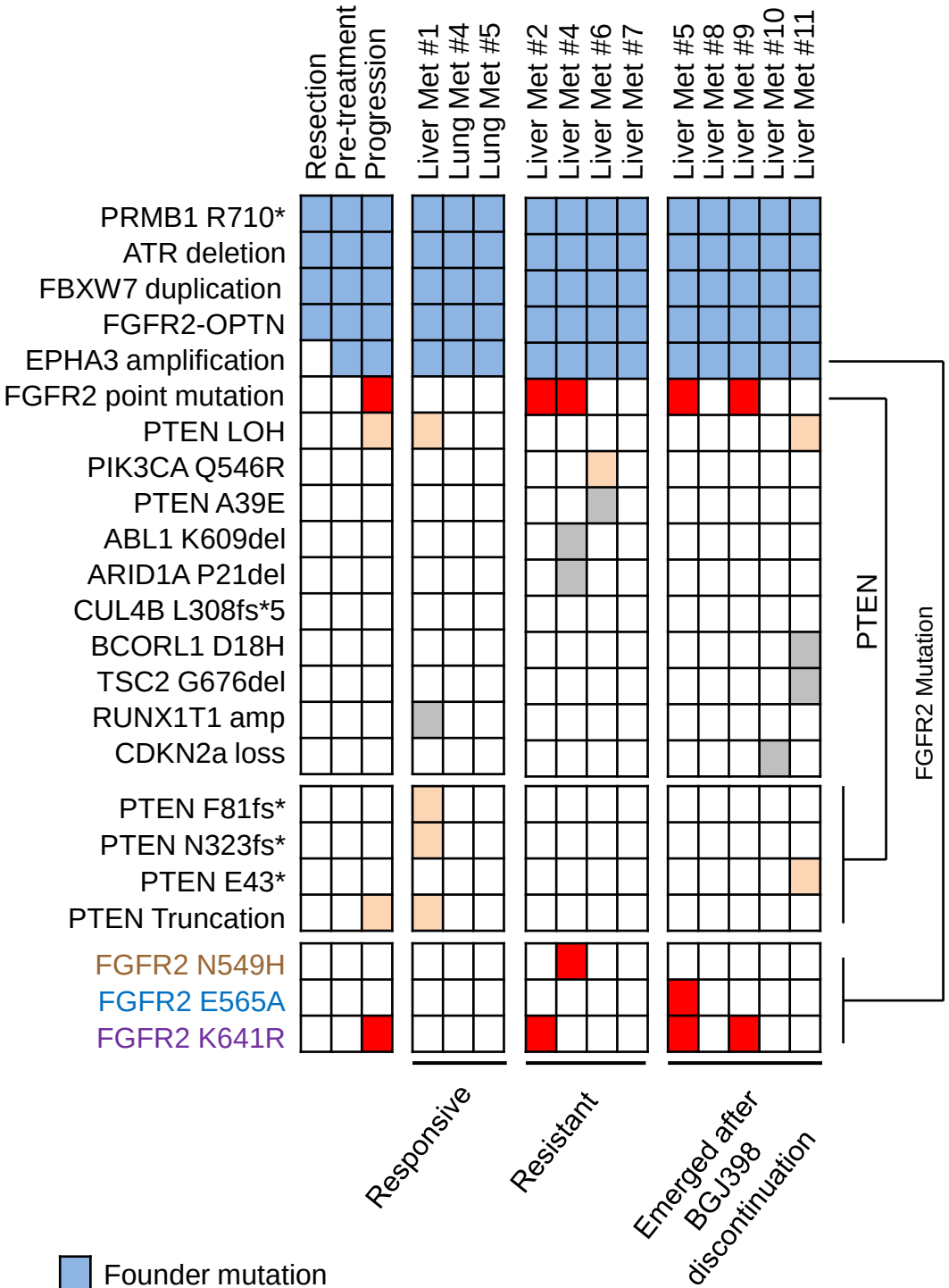

Supplementary Figure S3

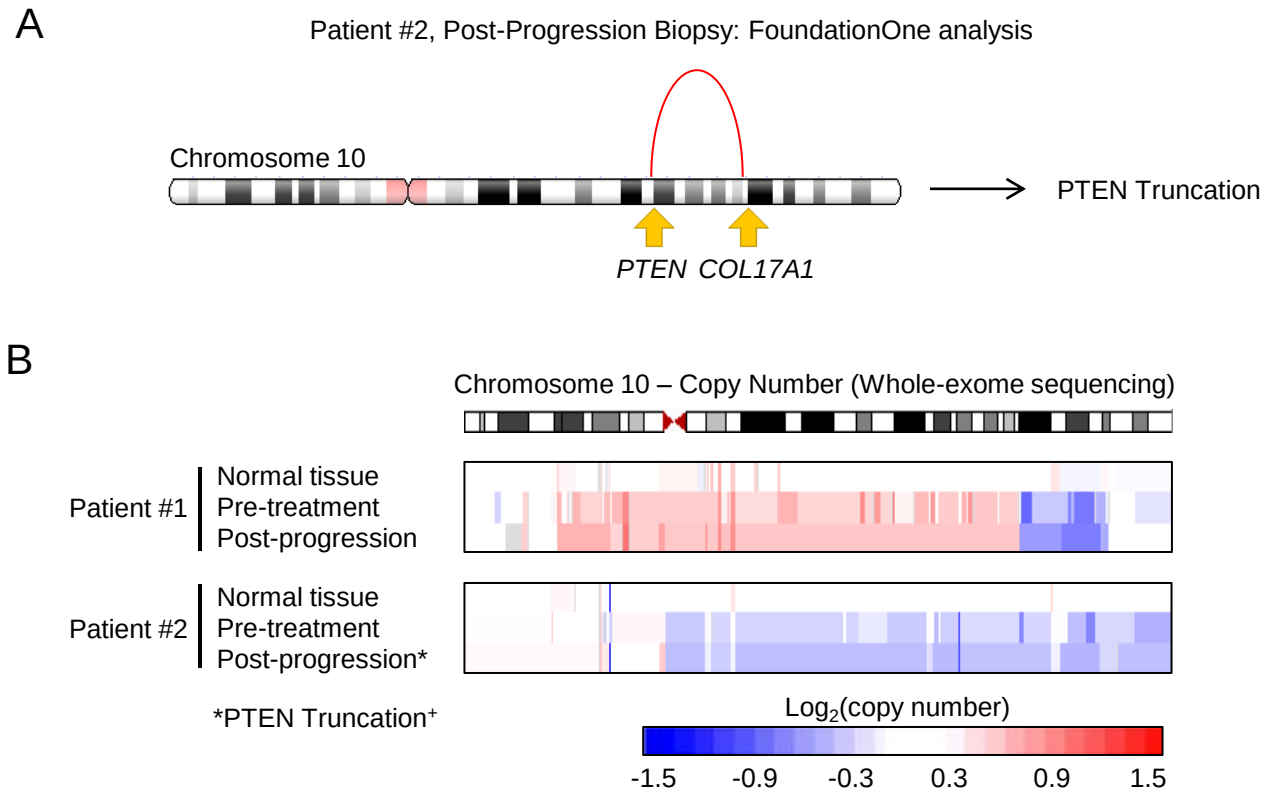

Supplementary Figure S4